



Staff, R. A., Hardiman, M., Bronk Ramsey, C., Adolphi, F., Hare, V. J., Koutsodendris, A. and Pross, J. (2019) Reconciling the Greenland ice-core and radiocarbon timescales through the Laschamp geomagnetic excursion. *Earth and Planetary Science Letters*, 520, pp. 1-9.

There may be differences between this version and the published version. You are advised to consult the publisher's version if you wish to cite from it.

<http://eprints.gla.ac.uk/187536/>

Deposited on: 31 May 2019

Enlighten – Research publications by members of the University of Glasgow_
<http://eprints.gla.ac.uk>

1 **RECONCILING THE GREENLAND ICE-CORE AND RADIOCARBON**
2 **TIMESCALES THROUGH THE LASCHAMP GEOMAGNETIC EXCURSION**

3

4 **Author affiliations:**

5 Richard A. Staff^{a,b*}, Mark Hardiman^c, Christopher Bronk Ramsey^b, Florian Adolphi^{d,e}, Vincent
6 J. Hare^{b,f}, Andreas Koutsodendris^g, Jörg Pross^{g,h}

7

8 ^a Scottish Universities Environmental Research Centre (SUERC), University of
9 Glasgow, Rankine Avenue, Scottish Enterprise Technology Park, East Kilbride G75 0QF, UK.

10 ^b Research Laboratory for Archaeology and the History of Art (RLAHA), University of
11 Oxford, Dyson Perrins Building, South Parks Road, Oxford OX1 3QY, UK. ^c Department of
12 Geography, University of Portsmouth, Buckingham Building, Lion Terrace,
13 Portsmouth PO1 3HE, UK.

14 ^d Climate and Environmental Physics, University of Bern, CH-3012 Bern, Switzerland.

15 ^e Department of Geology, Quaternary Sciences, Lund University, Sölvegatan 12, 22362 Lund,
16 Sweden.

17 ^f Department of Earth and Environmental Sciences, University of Rochester, Rochester, NY
18 14627, USA.

19 ^g Paleoenvironmental Dynamics Group, Institute of Earth Sciences, Heidelberg University, Im
20 Neuenheimer Feld 234, 69120 Heidelberg, Germany.

21 ^h Biodiversity and Climate Research Centre (BiK-F), Senckenberg, Senckenberganlage 25,
22 60325 Frankfurt, Germany.

23 * Corresponding author. Tel.: +44 (0)1355 270198.

24 E-mail address: richard.staff@glasgow.ac.uk (R.A. Staff)

25

26

- 27 **Keywords:**
- 28 Radiocarbon (^{14}C) dating
- 29 Beryllium-10 (^{10}Be)
- 30 Relative paleointensity
- 31 Laschamp geomagnetic excursion
- 32 Tenaghi Philippon, Greece
- 33 Campanian Ignimbrite (C.I.) tephra
- 34
- 35

36 **Abstract:**

37

38 Cosmogenic radionuclides, such as ^{10}Be and ^{14}C , share a common production signal,
39 with their formation in the Earth's upper atmosphere modulated by changes to the geomagnetic
40 field, as well as variations in the intensity of the solar wind. Here, we use this common
41 production signal to compare between the radiocarbon (IntCal) and Greenland ice-core
42 (GICC05) timescales, utilising the most pronounced cosmogenic production peak of the last
43 100,000 years – that associated with the Laschamp geomagnetic excursion circa 41,000 years
44 ago. We present 54 new ^{14}C measurements from a peat core ('TP-2005') from Tenaghi
45 Philippon, NE Greece, contiguously spanning between circa 47,300 and 39,600 cal. BP,
46 demonstrating a distinctive tripartite structure in the build up to the principal Laschamp
47 production maximum that is not present in the consensus IntCal13 calibration curve. This is
48 the first time that a continuous, non-reservoir corrected ^{14}C dataset has been generated over
49 such a long time span for this, the oldest portion of the radiocarbon timescale. This period is
50 critical for both palaeoenvironmental and archaeological applications, with the replacement of
51 Neanderthals by anatomically modern humans in Europe around this time. By placing our
52 Tenaghi Philippon ^{14}C dataset on to the Hulu Cave U-series timescale of Cheng et al. (2018)
53 via Bayesian statistical modelling, the comparison of TP-2005 ^{14}C with Greenland ^{10}Be fluxes
54 also implicitly relates the underlying U-series and GICC05 timescales themselves. This
55 comparison suggests that whilst these two timescales are broadly coherent, the IntCal13
56 timescale is likely some ~1000 years too old circa 40,000 cal. BP.

57

58

59 **1. Introduction**

60

61 Among the most pressing questions in palaeoenvironmental research today is the reliable
62 identification of synchronies or asynchronies of past climatic and environmental changes
63 across the globe. A fundamental problem in identifying such temporal relationships in
64 palaeorecords, however, is an inability to reliably compare inter-regional records beyond the
65 limits of chronological uncertainty.

66 Arguably, the best and most-widely cited record of palaeoclimatic change – the key
67 global reference ‘type site’ – is that provided by the Greenland ice-cores, due to their highly
68 resolved suite of multi-proxy palaeoenvironmental data (NGRIP members, 2004; Steffensen et
69 al., 2008), and their annual resolution, layer-counted chronology (Andersen et al., 2006;
70 Rasmussen et al., 2006; Svensson et al., 2008). Conversely, the most utilised geochronological
71 technique applied to late Quaternary palaeoenvironmental (and archaeological) sites elsewhere
72 in the world is provided by radiocarbon (^{14}C) dating (Brauer et al., 2014). However, in order to
73 compare data between the two timescales, one must assume that the respective ^{14}C and icecore
74 layer-counted chronologies are consistent – an assumption that must undoubtedly incorporate
75 uncertainties (Adolphi and Muscheler, 2016).

76 Here, we utilise the common production signal of the cosmogenic radionuclides ^{10}Be
77 (beryllium-10) and ^{14}C (radiocarbon) to link together the Greenland ice-core and radiocarbon
78 timescales for the oldest ~10,000 years of the radiocarbon timescale (i.e. the last ~50,000
79 years), taking advantage of the most pronounced cosmogenic production peak of the last
80 100,000 years – that associated with the Laschamp geomagnetic excursion circa 41,000 years
81 ago.

82

83

84 **1.1 Cosmogenic radionuclides and the Laschamp geomagnetic excursion**

85

86 Cosmogenic radionuclides, such as ^{10}Be and ^{14}C , are formed in the Earth's upper
87 atmosphere through the interaction of incoming high-energy cosmic rays with target nuclides
88 (Lal and Peters, 1967). The cosmic ray flux is modulated by both the shielding effect of the
89 Earth's magnetic field and the solar-induced interplanetary magnetic field (the 'solar wind').
90 The lower the strength of either the geomagnetic field or solar wind, the deflection of incoming
91 cosmic rays is reduced, and the production of cosmogenic radionuclides is therefore greater
92 (Elsasser et al., 1956).

93 The geomagnetic field exhibits long-term secular variation, including major reversals of
94 the Earth's magnetic (dipole) field between normal and reversed configurations, which occur
95 during periods of progressive decay in the Earth's dipole moment (Cox, 1969; Valet and
96 Meynadier, 1993). Additionally, shorter-term ($<10^4$ years) 'stability crises' occur whereby the
97 intensity of the geomagnetic field decreases more or less dramatically, but the field does not
98 undergo a long-term reversal. These may coincide with geomagnetic excursions – periods of
99 distorted dipole geometry when the virtual geomagnetic poles (VGPs) move away from the
100 area of normal high-latitude secular variation – or even short-term (10^2 - 10^3 years) complete
101 reversals (where VGPs temporarily migrate to higher latitudes of the opposite hemisphere)
102 (Nowaczyk et al., 2012). The most prominent of these geomagnetic excursions over the past
103 100,000 years is known as the 'Laschamp event', dated to circa 41,000 years ago (Bonhommet
104 and Babkine, 1967; Guillou et al., 2004; Singer et al., 2009). This event is characterised by a
105 short-term full reversal of the geomagnetic field (Nowaczyk et al., 2012) and the lowest
106 geomagnetic field intensities of the past 100,000 years, falling to approximately 10% of today's
107 value (Laj et al., 2000; Nowaczyk et al., 2013).

108 Such geomagnetic events can provide global, temporally synchronous signals in
109 palaeoenvironmental archives, observable directly in records of relative palaeointensity, as well
110 as in records of cosmogenic nuclides (including ^{10}Be and ^{14}C). Thus, it is theoretically possible

111 to link palaeoenvironmental archives using these isochronous signals (Brauer et al., 2014). ^{10}Be
112 has a short (1-2 year) atmospheric residence time (McHargue and Damon, 1991), providing an
113 excellent record of past cosmogenic nuclide production variation, and has been measured
114 directly in the Greenland ice-cores (Yiou et al., 1997; Muscheler et al. 2004) (unlike ^{14}C , which
115 is too low in abundance to detect within the ice). ^{14}C provides a less direct production marker,
116 however, because of its incorporation into the global carbon cycle system and consequent
117 exchanges between the global carbon reservoirs, thus complicating the intercomparison of such
118 records.

119

120

121 **1.2 The Greenland ice-core chronology**

122

123 The Greenland ice-core chronology ‘GICC05’ is the most recent timescale applied to the
124 Greenland ice-cores, tying together the GRIP (Johnsen et al. 1992), GISP2 (Grootes et al.,
125 1993), NGRIP (NGRIP members, 2004) and NEEM (NEEM Community Members, 2013)
126 records (Seierstad et al., 2014). For the entire time period covered by the ^{14}C dating technique,
127 i.e., the last circa 50,000 years, GICC05 is based on direct counting of the annual layers within
128 the ice (Andersen et al., 2006; Rasmussen et al., 2006; Svensson et al., 2008; Brauer et al.,
129 2014). The uncertainty on the timescale is based upon the ‘maximum counting error’ (MCE)
130 concept, whereby each uncertain layer is counted as $\frac{1}{2} \pm \frac{1}{2}$ year and added linearly. Thus,
131 throughout the Last Glacial period, the MCE on GICC05 amounts to approximately 5%. It
132 should be noted that GICC05 uses the notation ‘b2k’ – i.e., ‘calendar years before its datum,
133 AD 2000’ – whereas herein we convert this to years ‘BP’ (before present, AD 1950), enabling
134 more direct comparison with the Hulu Cave uranium (U-)series and IntCal13 timescales
135 (below).

136 Since its introduction in 2005, GICC05 has now been utilised for over a decade,
137 demonstrating the robustness of the chronology, though there have been recent suggestions of
138 small scale errors. For example, Sigl et al. (2015) presented evidence, making use of the
139 distinctive ‘AD 775 and 994 events’ recorded as both ^{10}Be and ^{14}C production spikes, as well
140 as using tephra marker horizons, that the ice-core chronology is 7 years too old by the late first
141 millennium AD. Over a longer time range, Buizert et al. (2015) presented evidence that
142 GICC05, on average, misses 6.3 out of every 1,000 annual layers. This conclusion is based
143 upon comparison of the respective oxygen isotope ($\delta^{18}\text{O}$) records of the NGRIP ice-core and
144 Hulu Cave (China) speleothem, which is independently U-series dated. However, this
145 comparison of $\delta^{18}\text{O}$ records assumes synchronicity of the respective palaeoclimatic signals –
146 an assumption that may not necessarily hold true (Lane et al., 2013; Brauer et al., 2014).

147

148

149 **1.3 Radiocarbon dating and the IntCal timescale**

150

151 In order to generate meaningful ages from the ^{14}C dating method, a calibration stage is
152 required since the concentration of ^{14}C (relative to stable ^{12}C and ^{13}C) in the environment
153 changes through time. This is the result of both the variations in production rate (Lal and Peters,
154 1967) outlined above and carbon cycle effects, which alter the global distribution of relatively
155 older or younger carbon sources between the respective reservoirs of Earth’s carbon cycle
156 system through time (Broecker et al., 1960; Siegenthaler et al., 1980).

157 Calibration involves the comparison of samples’ raw isotopic measurements with the
158 internationally ratified, consensus radiocarbon calibration curve ‘IntCal13’ (Reimer et al.,
159 2013), which itself is comprised of ‘known age’ material from a variety of palaeo-archives. For
160 the last ~12,500 years, the IntCal curve is composed of independently dendro-chronologically

161 dated wood. Previous research (Muscheler et al., 2004, 2008, 2014a; Adolphi and Muscheler,
162 2016) has utilised this high-resolution, continuous record of past variation in atmospheric ^{14}C
163 concentrations ($\Delta^{14}\text{C}$) to tie this most recent period of the IntCal timescale to the ^{10}Be signal in
164 Greenland. These authors found an offset of approximately 65 years between GICC05 and
165 IntCal during the Preboreal (i.e. circa 12,500 to 10,000 years ago), with GICC05 seemingly
166 including a small over-count – an offset consistent in scale with that proposed by Sigl et al.
167 (2015). Since this latest portion of the ^{14}C calibration curve is composed of robustly
168 dendrochronologically dated records, Muscheler et al. (2008) attributed this 65 year offset to
169 uncertainties in the ice-core layer counting.

170 Further back in time, through to the methodological limit of radiocarbon dating (circa
171 50,000 years ago), however, the ^{14}C calibration curve is less certain. The central archive for
172 this earlier period is that provided by plant macrofossils picked from the annually laminated
173 sediments of Lake Suigetsu, Japan (Staff et al., 2011; Bronk Ramsey et al., 2012). Additional
174 data are provided by speleothems (Hoffmann et al., 2010; Southon et al., 2012), marine corals
175 (e.g. Fairbanks et al., 2005), and foraminifera from marine sediment cores (e.g. Hughen et al.,
176 2006), all of which incorporate (marine- or dead carbon) ‘reservoir effects’ that require
177 correction and thereby introduce additional uncertainties. These reservoir effects would also be
178 expected to ‘smooth’ the atmospheric $\Delta^{14}\text{C}$ signal, making comparison to ^{10}Be records more
179 complicated. Unlike these latter records, the Lake Suigetsu data provide a direct record of
180 atmospheric $\Delta^{14}\text{C}$, and have previously been used to compare to both records of
181 palaeomagnetic intensity (e.g. Nowaczyk et al., 2013) and to ^{10}Be in the Greenland ice-cores
182 (e.g. Bronk Ramsey et al., 2012; Muscheler et al., 2014b). However, the Lake Suigetsu data are
183 necessarily discontinuous – limited by the stochastic finds of plant macrofossil remains in the
184 sediment profile – as well as being potentially less reliable due to the methodological problems
185 associated with dating such small samples close to the radiocarbon detection limit (Muscheler

186 et al., 2014b). As with the Greenland ice-cores (above), the Lake Suigetsu dataset also has
187 relatively large cumulative counting uncertainties by ~40,000 years BP.

188 The promise of more reliable, continuous data for this older time period comes from
189 floating tree-ring sequences, most notably long-lived New Zealand kauri (*Agathis australis*)
190 (Turney et al., 2010, 2016; Hogg et al., 2013). Such records are limited in duration, however,
191 by the up to ~2,000 year life-spans of individual trees, limiting their utility for comparison to
192 the Greenland ^{10}Be record to relatively short periods of time (Muscheler et al., 2014b; Turney
193 et al., 2016). Recently, Muscheler et al. (2014b) presented such a comparison, arguing that the
194 Greenland ice-core and ^{14}C (IntCal) timescales were discordant circa 40,000 years ago, with
195 the calibrated ^{14}C timescale apparently 1,200 years too old. This would be a highly significant
196 finding, if true, since it compromises the inter-comparison of ^{14}C -dated palaeoenvironmental
197 records with those dated by other methods. It also directly affects the interpretation of ^{14}C data
198 through this time period across other disciplines, such as archaeological applications, with the
199 replacement of Neanderthals by anatomically modern humans in Europe around this time
200 (Higham et al., 2014). However, the study of Muscheler et al. (2014b) was necessarily limited
201 to a short record (1,350 years), minimising the $\Delta^{14}\text{C}$ structure that could be compared with the
202 equivalent ^{10}Be -inferred signal, and thereby reducing the reliability of the correlation drawn.
203 Recently, Cheng et al. (2018) have provided an extended record from Hulu Cave (China) based
204 upon radiocarbon data from two new speleothems ('MSD' and 'MSL'), adding to the
205 previously published dataset of Southon et al. (2012) from speleothem 'H82' which covered
206 the period ~10.7 to 26.9 ka BP. As with the Lake Suigetsu dataset (above), this new Hulu Cave
207 record now extends across the entirety of the radiocarbon dating method. The latter has the
208 advantage of a highly precise U-series derived calendar age scale, and will provide the central
209 archive of the next iteration of the consensus calibration curve, IntCal (Reimer et al., in prep.,
210 Radiocarbon).

211 As noted above, speleothems incorporate a reservoir effect, which requires correction,
212 and therefore introduces further uncertainty into the ^{14}C values. Southon et al. (2012) and
213 Cheng et al. (2018) both describe the “unusually small and stable” (450 ± 70 ^{14}C years) ‘dead
214 carbon fraction’ (DCF) registered in these Hulu Cave speleothems, which makes them
215 particularly attractive for radiocarbon calibration purposes. However, it would seem that this
216 small and stable DCF is a result of the unique geological setting of the site, such that the ‘inbuilt
217 age’ recorded by the speleothem dripwater is more of a ‘soil reservoir effect’, rather than a
218 DCF, *sensu stricto*. The consequence of this is the favourable low and stable ‘DCF’; however,
219 the pay-off is that the atmospheric ^{14}C signal is effectively smoothed at this resolution (~450
220 years), meaning that higher frequency signal is consequently lost.

221 Thus, there are both strengths and weaknesses in all of the aforementioned calibration
222 records. To add to this current state of knowledge, therefore, we herein exploit new ^{14}C data
223 from a continuous peat sequence from Greece, extending over a significantly longer time period
224 (circa 47,300 to 39,600 cal. BP) than the kauri dataset utilised by Muscheler et al. (2014b). This
225 enables us to use the entirety of the $\Delta^{14}\text{C}$ signal associated with the build-up to- and peak of
226 the Laschamp excursion to enable more robust comparison of the calibrated ^{14}C and Greenland
227 ice-core time scales. Our dataset also provides a direct record of atmospheric ^{14}C concentration,
228 unlike the Hulu Cave speleothems, and provides continuous material for ^{14}C dating, unlike the
229 stochastic Lake Suigetsu dataset, without the issues of small sample sizes associated with the
230 latter record. The drawback of our new dataset, however, is the lack of independent chronology,
231 which we necessarily need to obtain through Bayesian statistical modelling (section 3.2,
232 below).

233

234

235 2. Study site

236

237 Tenaghi Philippon is situated in the Philippi peatland within the Drama Basin of NE
238 Greece (Fig. 1). Since its discovery and initial exploitation in the 1960s, the site has become
239 widely recognised as harbouring one of the best terrestrial archives of Quaternary climatic and
240 environmental change in Europe (Wijmstra, 1969; Tzedakis et al., 2006; Pross et al., 2015 and
241 refs. therein). Scientific drilling campaigns at the site have yielded a peat-dominated sequence
242 that extends to a depth of nearly 200 m and covers the last ~1.35 Ma continuously. This
243 sequence represents an extremely sensitive recorder of rapid climatic change both during
244 glacial and interglacial boundary conditions, which is ascribed to the site's intermediate
245 position between higher-latitude (i.e., North Atlantic Oscillation- and Siberian Highinfluenced)
246 and lower-latitude (monsoonally influenced) climatic regimes, its intramontane setting, and its
247 proximity to the glacial refugia of thermophilous plant taxa (Pross et al., 2009, 2015).

248 In 2005, a new, 60 m long core ('TP-2005'; 40°58'24" N, 24°13'26" E, 40 m asl) was
249 recovered from Tenaghi Philippon (Pross et al., 2007). The core consists primarily of fen peat
250 and is believed to represent continuous accumulation throughout the last circa 310 kyrs
251 (Fletcher et al., 2013). A previous study (Müller et al., 2011) presented 20 accelerator mass
252 spectrometry (AMS) ¹⁴C dates, spanning the majority of the approximately 50,000 year ¹⁴C
253 dating time period, from the uppermost 15.28 m of the TP-2005 core (Table S1). Additionally,
254 three tephra layers have been identified at 7.61 m, 9.70 m and 12.64-12.87 m core depths, and
255 respectively geochemically correlated to the Y-2 tephra (resulting from the Cape Riva eruption
256 of Santorini), Y-3 tephra (resulting from an eruption from the Campi Flegrei), and Y-5 tephra
257 (from the regionally widespread Campanian Ignimbrite eruption, also from the Campi Flegrei)
258 (Müller et al., 2011; Albert et al., 2015 Pross et al., 2015; Wulf et al., 2018). Accompanying

259 palaeoenvironmental data are provided by a centennial resolution pollen record spanning
260 Marine Isotope Stages (MIS) 4 to 2 (Müller et al., 2011).

261

262

263 **3. Methods**

264

265 3.1 Radiocarbon dating

266

267 Contiguous peat sub-samples (maximum 5 cm thick) from Tenaghi Philippon core
268 ‘TP2005’ were taken from 12.87 to 14.80 cm depth – i.e. spanning the time period immediately
269 preceding the deposition of the visible Campanian Ignimbrite (C.I.) tephra, back to the
270 methodological limit of ^{14}C dating (circa 50,000 cal. BP). Each sub-sample was physically
271 homogenised prior to a standard acid-base-acid (ABA) chemical pre-treatment for radiocarbon
272 dating, following the method of Brock et al. (2010). The three main stages of this process
273 (successive acid-, base-, and acid washes) are similar across most radiocarbon laboratories and
274 are respectively intended to remove: (i) sedimentary- and other carbonate contaminants; (ii)
275 organic (principally humic- and fulvic-) acid contaminants; and (iii) any dissolved atmospheric
276 CO_2 that might have been absorbed during the preceding base wash. In this way, any potential
277 secondary carbon contamination is removed, leaving the samples pure for subsequent
278 combustion, graphitisation and accelerator mass spectrometry (AMS) ^{14}C dating. At the Oxford
279 Radiocarbon Accelerator Unit (ORAU) ABA chemical pre-treatment of peat samples
280 (laboratory pre-treatment code ‘VV’) involves successive 1 M HCl (20 mins, 80 °C), 0.2 M
281 NaOH (20 mins, 80 °C) and 1 M HCl (1 hr, 80 °C) washes, with each stage followed by rinsing
282 (≥ 3 times) with ultrapure MilliQ™ deionised water. From five samples, the base-soluble humic
283 acid component extracted from the peat was additionally dated to provide supporting

284 information on the likely contribution of mobile- (presumably, downward-percolating young-
285) contaminant to the primary base-insoluble ('humin') component of the peat samples.
286 Specifically, this involved the collection of the base-soluble fraction of these samples and
287 reacidification through the addition of 1 M HCl, followed by centrifugation and rinsing (twice)
288 with ultrapure MilliQ™ deionised water (ORAU laboratory pre-treatment code 'HW'). AMS
289 ¹⁴C dating was subsequently performed on the 2.5 MV HVEE tandem AMS system at ORAU
290 (Bronk Ramsey et al., 2004; Staff et al., 2014).

291

292

293 3.2 Chronological modelling

294

295 The TP-2005 ¹⁴C data were analysed with the Bayesian statistical software OxCal ver.
296 4.3 (Bronk Ramsey, 2019), implementing a Poisson-process ('P_Sequence') deposition
297 model (Bronk Ramsey, 2008). The P_Sequence model takes into account the complexity
298 (randomness) of the underlying peat accumulation process, and thus provides the most realistic
299 age-depth model for the TP-2005 peat profile on the calibrated radiocarbon timescale. For
300 comparison purposes, we herein modelled our TP-2005 ¹⁴C data on to both the recently
301 published Hulu Cave dataset of Cheng et al. (2018), as well as the current consensus (IntCal)
302 calibration curve (Reimer et al., 2013). The rigidity of each P_Sequence (i.e., the regularity
303 of the peat accumulation rate) is determined iteratively within OxCal through a model
304 averaging approach, based upon the likelihood (i.e., calibrated ¹⁴C) data included within the
305 model (Bronk Ramsey and Lee, 2013). 'Boundary' functions were applied at the top and
306 bottom of the 'P_Sequence' (at 12.87 m and 14.80 m core depth, respectively) – the former
307 providing a modelled, ¹⁴C-derived age for the C.I. tephra. Objective outlier analysis was applied
308 to down-weight any statistically anomalous data points (Bronk Ramsey, 2009; Bronk

309 Ramsey et al., 2010). An ‘r-type’ **Outlier_Model** was selected, allowing for short-term
310 fluctuations in the ^{14}C concentrations between the respective radiocarbon reservoirs of the
311 Tenaghi Philippon, Hulu Cave and IntCal13 datasets. (N.b., a premise of this paper is that the
312 IntCal and Hulu Cave curves currently smooth out real, higher frequency ‘wiggles’ in
313 atmospheric radiocarbon concentration, $\Delta^{14}\text{C}$ – i.e., that the datasets have short-term offsets in
314 their apparent ^{14}C concentrations compared to the TP-2005 record – which is allowed for by
315 the r-type **Outlier_Model**.) A prior ‘**Outlier**’ probability of 5% was applied to all of the
316 TP-2005 ^{14}C determinations, since there was no reason, *a priori*, to believe that any samples
317 were more likely to be statistical outliers than others. As noted, both the Hulu Cave (Cheng et
318 al., 2018) and IntCal13 ^{14}C calibration curve (Reimer et al., 2013) were used, with alternative
319 comparison datasets from Lake Suigetsu (Bronk Ramsey et al, 2012), Bahamas speleothem
320 (Hoffmann et al., 2010), and Cariaco Basin foraminifera (Hughen et al., 2006) plotted for
321 comparison purposes only. The coding of these primary deposition models and the model
322 output are given in the Supplementary Material (S1 and Tables S3 and S4).

323 Similar Poisson-process modelling was applied to the original TP-2005 ^{14}C
324 determinations of Müller et al. (2011), using two successive **P_Sequences** for the lower and
325 upper core sections, cross-referencing the upper **Boundary** of the lower **P_Sequence**
326 (12.87m core depth; the lower contact of the C.I. tephra) to equal the lower **Boundary** of the
327 upper **P_Sequence** (12.64m core depth; the upper contact of the C.I. tephra). Again, the
328 model coding is given in the Supplementary Material (S2).

329 One consideration with the **P_Sequence** deposition model is that it produces an
330 inevitable attenuation of the authentic $\Delta^{14}\text{C}$ maxima and minima by ‘pulling’ the data to more

^{14}C production rates using the production rate model of Herbst et al. (2017) and the Local
Interstellar Spectrum of Potgieter et al. (2014), assuming a constant solar modulation potential

331 closely fit the Hulu Cave or IntCal calibration datasets. Therefore, supporting age-depth models
332 were subsequently generated in OxCal, simply applying a uniform ('U_Sequence')
333 deposition model (Bronk Ramsey, 2008), rather than the P_Sequence. The coding of these
334 supporting deposition models is also given in the Supplementary Material (S3), as is the model
335 output (Tables S3 and S4). In reality, the two differing model assumptions (P_Sequence or
336 U_Sequence) produce similar output (Figs. S1 and S2), reflecting the insensitivity of our
337 conclusions presented herein to the choice of chronological model construction.

338

339

340 3.3. $\Delta^{14}\text{C}$ modelling from GRIP ^{10}Be fluxes and Black Sea and GLOPIS-75 VADM

341

342 GRIP ^{10}Be fluxes (Yiou et al., 1997; Muscheler et al., 2004) and estimates of the Earth's virtual
343 axial dipole moment (VADM) from both the individual Black Sea record (Nowaczyk et al.,
344 2012, 2013) and the GLOPIS-75 stack (Laj et al., 2004, 2014) were converted into $\Delta^{14}\text{C}$ using
345 previously applied methods (Muscheler et al., 2004, 2005). First, VADM was converted into
346 ($\sim 300\%$ between 48,000 and 40,000 cal.BP), we ran the carbon cycle model with slightly
347 reduced ocean diffusivity (70% of the preindustrial value, resembling reduced ocean ventilation

of 800 MeV that resembles the modern average solar activity (Muscheler et al., 2016). In a
second step, $\Delta^{14}\text{C}$ was modelled from GRIP ^{10}Be fluxes and VADM-based ^{14}C production rates
using a box-diffusion carbon cycle model (Siegenthaler et al., 1980; Muscheler et al., 2004).
We assume a $^{10}\text{Be}/^{14}\text{C}$ production rate ratio of 1:1 which is in agreement with $^{10}\text{Be}/^{14}\text{C}$
comparisons from the Holocene (Adolphi and Muscheler, 2016) as well as production rate
models (Herbst et al., 2017). To match the amplitude of the overall $\Delta^{14}\text{C}$ increase in IntCal

348 in the Glacial) and reduced air/sea exchange rates (75% of the preindustrial value, resembling
349 increased sea ice extent). Note, that this only affects the overall amplitude of the modelled $\Delta^{14}\text{C}$
350 change, but not the shape of the curve, since these parameters were kept constant over the entire
351 timeframe.

352

353

354 **4. Results**

355

356 Our 54 new ^{14}C determinations from TP-2005 are presented in Table S2 and, having been
357 modelled against both the Hulu Cave dataset and IntCal13 (see section 3.2, above), are plotted
358 against depth in Fig. 2. These new data suggest that the previous ^{14}C -based chronology of
359 Müller et al. (2011) underestimated the true age of the peat sequence for the time period before
360 circa 39,000 cal. BP; this may be due to insufficient chemical pre-treatment to remove
361 (young/modern) contaminant carbon, which has an increasing influence on ^{14}C measurements
362 with increasing age.

363 The inferred $\Delta^{14}\text{C}$ values from our new TP-2005 data show three periods of increasing
364 $\Delta^{14}\text{C}$ values (Fig. 3). On the Hulu Cave U-series timescale these successive increases occur
365 from circa 47,300 cal. BP to 45,600 cal. BP, reaching a maximum of approximately 450‰;
366 from circa 44,900 cal. BP to 43,700 cal. BP, reaching a maximum of approximately 400‰;
367 and from circa 43,200 cal. BP to 42,000 cal. BP, reaching a maximum of approximately 650‰.
368 This final elevation represents the peak of the Laschamp geomagnetic excursion in TP-2005,
369 and continues until at least the timing of the Campanian Ignimbrite (C.I.) tephra, dated to circa
370 39,600 cal. BP (Fig. 4), interrupted by a(t least one) depression in $\Delta^{14}\text{C}$ values between circa
371 41,000 and 40,400 cal. BP.

372

373

374 **5. Discussion**

375

376 An initial observation is that our new TP-2005 data provide no evidence for the extremely
377 high $\delta^{14}\text{C}$ values associated with the Laschamp geomagnetic excursion that have been
378 suggested by some previous studies (e.g. Voelker et al., 2000; Hughen et al., 2006; Hajdas et
379 al., 2011). There are also no data identified as being statistical outliers (Bronk Ramsey, 2009;
380 Bronk Ramsey et al., 2010), demonstrating the integrity of the peat sequence both for
381 reconstructing past variation in $\delta^{14}\text{C}$ as well as for palaeoenvironmental research. We note that
382 the age-depth profile for TP-2005 is more linear (especially at the younger end) when modelled
383 on to the Hulu Cave dataset rather than the IntCal13 curve (Fig. 2), which implies greater
384 congruence of the TP-2005 ^{14}C data with the Hulu Cave record (Cheng et al., 2018) rather than
385 IntCal13 (Reimer et al., 2013).

386 Our new data (Fig. 3) show higher frequency $\delta^{14}\text{C}$ variability than the ‘smoothed’
387 IntCal13 curve, which inevitably loses authentic signal when the contributing ^{14}C datasets are
388 averaged into the consensus curve (Reimer et al., 2013; Fig. S4). The ^{14}C data from the two
389 individual, non-reservoir corrected atmospheric ^{14}C datasets (TP-2005 and Lake Suigetsu)
390 match each other within the bounds of statistical uncertainty. The Lake Suigetsu dataset shows
391 higher frequency variability, however. One reason for this is the ~150 year smoothing of the
392 TP-2005 data (due to the contiguous sub-sampling methodology applied), as compared to the
393 annual signal contained within the individual Japanese terrestrial plant macrofossil samples.
394 The other reason is the statistical ‘noise’ in the Lake Suigetsu data, which is the result of the
395 methodological problems of dating very small individual plant macrofossil samples so close to
396 the limit of ^{14}C detection (Muscheler et al., 2014b). For this latter reason, we prefer the TP2005
397 dataset (as compared to the Lake Suigetsu record) as more reliably representing the authentic

398 signal in past variability of atmospheric radiocarbon concentration for this earliest portion of
399 the ^{14}C time frame. We also reiterate that our TP-2005 data demonstrate a direct atmospheric
400 signal, therefore avoiding the additional uncertainties associated with the reservoir effects of
401 either the marine or speleothem datasets. The tripartite structure seen in the Tenaghi Philippon
402 data also demonstrates higher amplitude shifts in the build-up to the principal Laschamp peak
403 than the Hulu Cave dataset. As noted above (section 1.3), we suggest that this attenuation in
404 the Hulu Cave record is the result of the longer ~ 450 year smoothing effect of the soil reservoir
405 effect at the site.

406 However, since the TP-2005 data have necessarily been modelled on to the Hulu Cave
407 and IntCal13 timescales (see section 3.2), such errors currently contained within these
408 calibration datasets will propagate through into the placement of our TP-2005 data in calendar
409 time and hence on the amplitude of the reconstructed $\Delta^{14}\text{C}$. That said, the general shape of the
410 $\Delta^{14}\text{C}$ data will be largely unaffected by this process and, consequently, we can compare TP2005
411 $\Delta^{14}\text{C}$ to the equivalent signal inferred from Greenland ^{10}Be to assess the concordance (or lack
412 thereof) between the underlying Hulu Cave (U-series), IntCal, and Greenland ice-core
413 (GICC05) timescales themselves.

414 Significantly, the general shape of the TP-2005 $\Delta^{14}\text{C}$ data, consisting of three successive
415 rises in atmospheric ^{14}C concentration in the $\sim 6,000$ years leading up to the peak values
416 associated with the Laschamp geomagnetic excursion (from circa 42,000 cal. BP in the TP2005
417 record), broadly tracks equivalent increases calculated from ^{10}Be flux measured in the
418 GRIP ice-core (Yiou et al., 1997; Muscheler et al., 2004, 2014b) (Fig. 3). This is the first time
419 that this clear, tripartite structure in $\Delta^{14}\text{C}$ has been directly observed in the build-up to the
420 Laschamp excursion.

421 We can additionally compare our record with estimates of the Earth's dipole moment
422 (virtual axial dipole moment, VADM) obtained from relative palaeointensity studies, to
423 provide assessment of the role of the geomagnetic field in contributing to cosmogenic
424 radionuclide production. To this end, we utilise both the Black Sea sediment record of
425 Nowaczyk et al. (2013), drilled ~1000 km East of Tenaghi Philippon, as well as the GLOPIS75
426 globally-averaged curve (Laj et al., 2004, 2014). The Black Sea dataset is not truly independent,
427 in that it has been tuned to the GICC05 timescale using palaeoenvironmental proxy data from
428 the two archives (Nowaczyk et al., 2012). Likewise, the GLOPIS-75 dataset is composed of
429 records aligned on to a single timescale (Laj et al., 2004, 2014). However, the inferred $\Delta^{14}\text{C}$
430 from both of these records closely mimics the variations evident in the Greenland ^{10}Be -inferred
431 $\Delta^{14}\text{C}$ in both structure and amplitude, and also shares similar characteristics with the TP-2005
432 $\Delta^{14}\text{C}$ data from Tenaghi Philippon (Fig. 3).

433 Despite this general coherence in the $\Delta^{14}\text{C}$, ^{10}Be , and palaeomagnetic intensity records,
434 there are also distinct differences evident. Firstly, the amplitude of the successive $\Delta^{14}\text{C}$
435 increases is vastly different in the ^{10}Be and VADM-inferred data, as compared to the TP-2005
436 dataset. And, whilst ^{10}Be and VADM indicate that the first two $\Delta^{14}\text{C}$ increases are about a
437 factor of three smaller than the final rise circa 42,500 to 40,000 cal. BP, the initial two $\Delta^{14}\text{C}$
438 maxima in TP-2005 (as modelled on to the Hulu Cave dataset) are approximately $\frac{2}{3}$ the
439 amplitude of the final Laschamp peak (Fig. 3d). When instead modelled on to IntCal13 (Fig.
440 3e), the TP-2005 data show a comparable magnitude $\Delta^{14}\text{C}$ increase for all three steps, which
441 clearly accords less well with the ^{10}Be and VADM-inferred signals. This is another line of
442 argument in support of the Hulu Cave dataset as providing the more accurate $\Delta^{14}\text{C}$ record
443 through this time interval compared to the current consensus calibration curve (IntCal13).

444 In terms of timing, the earliest $\delta^{14}\text{C}$ maximum (circa 45,600 cal. BP) in TP-2005, as
445 modelled on to the Hulu Cave U-series timescale, is represented by concomitant increases in
446 both the Greenland ^{10}Be and Black Sea palaeointensity-inferred $\delta^{14}\text{C}$ records. However, the
447 second $\delta^{14}\text{C}$ maximum (circa ~~46,000~~ 43,700 cal. BP) does not demonstrate such a correlation
448 to the ^{10}Be or VADM-inferred records. Conversely, the third and final increase in TP-2005
449 $\delta^{14}\text{C}$ to the principal Laschamp peak does appear similar in structure to the ^{10}Be and
450 VADM-inferred records, with an interruption to the rising $\delta^{14}\text{C}$ trend circa 42,800 cal. BP
451 evident in all of the records, before a resumption of increasing values up to the principal
452 Laschamp production maximum. Again, we see a better fit of our TP-2005 data against these
453 alternative ^{10}Be and palaeointensity-inferred $\delta^{14}\text{C}$ records when modelled on to the Hulu Cave
454 dataset rather than IntCal13 (Fig. 3). This is likely due to the IntCal13 curve containing
455 incorrect structure, particularly around the timing of the principal Laschamp peak itself. This
456 is unsurprising since the constituent datasets of IntCal13 are themselves in disagreement at this
457 time (Fig. S4). It would appear that the DCF of the independently U-series dated Bahamas
458 speleothem record (Hoffmann et al., 2010) is being over-corrected at this time. Conversely, the
459 $\delta^{14}\text{C}$ of the Cariaco Basin dataset (Hughen et al., 2006) appears too high, and it is likely that
460 errors in either the marine reservoir correction or, more likely, the climatically wiggle-matched
461 timescale of this latter record is responsible for the erroneous structure in IntCal at this time.

462 As noted above, the second maximum in the TP-2005 $\delta^{14}\text{C}$ data circa 43,700 cal. BP is
463 not represented by equivalent signal in the ^{10}Be or VADM-inferred datasets. We therefore
464 hypothesise that the signal evident in the direct (TP-2005) $\delta^{14}\text{C}$ record at this time is the result
465 of processes internal to the global carbon cycle. We note that, as with all such radiocarbon
466 calibration datasets, firm conclusions should not be drawn until corroboration is provided from
467 further archives. Such support is provided for the subsequent $\delta^{14}\text{C}$ minimum, however, with

468 an equivalent minimum seen in the New Zealand kauri record of Turney et al. (2010; which
469 was also utilised by Muscheler et al. 2014b) when that record is also modelled on to the Hulu
470 Cave dataset. Interestingly, a similar interruption to the longer-term $\delta^{14}\text{C}$ increase to the
471 principal Laschamp $\delta^{14}\text{C}$ maximum is also seen in both the TP-2005 and kauri records circa
472 42,800 cal BP, providing further corroboration for the authenticity of this signal.

473 One further difference between the structure of the TP-2005 and Greenland ^{10}Be -inferred
474 $\delta^{14}\text{C}$ occurs in the aftermath of the principal Laschamp peak. Whereas the ^{10}Be data show a
475 steady decline from circa 41,000 to 39,000 cal. BP, the TP-2005 $\delta^{14}\text{C}$ data exhibit an initial,
476 equivalent decline (which is not seen in the Hulu Cave or IntCal13 datasets; Fig. S4), but then
477 return to higher $\delta^{14}\text{C}$ values again at around 40,200 cal. BP. Similar structure is hinted at in the
478 Lake Suigetsu record; however, it remains unclear as to how much of the higher frequency
479 signal in the Suigetsu record is genuine and how much is noise. The lack of a comparable signal
480 in the ^{10}Be flux suggests that, if genuine, this $\delta^{14}\text{C}$ signal would also be related to processes
481 internal to Earth's carbon cycle. Even more speculatively, we note the approximate coincidence
482 of this return to higher $\delta^{14}\text{C}$ with Heinrich Stadial 4, during which the Atlantic Meridional
483 Overturning Circulation (AMOC) is believed to have been significantly reduced in strength
484 (Böhm et al., 2015; Eggleston et al., 2016). The AMOC reduction would have less efficiently
485 removed relatively ^{14}C -enriched CO_2 from the atmosphere and less efficiently returned
486 relatively ^{14}C -depleted CO_2 from the deep ocean. Therefore, there is a theoretical expectation
487 that $\delta^{14}\text{C}$ would increase at about this time, which would not be seen in the ^{10}Be and
488 VADMinferred records. The afore-mentioned period of divergence in $\delta^{14}\text{C}$ and ^{10}Be circa
489 43,800 cal.

490 BP does not coincide with a Heinrich Stadial, but it does coincide with a ‘non-Heinrich’ Stadial
491 (Greenland Stadial 12), which we again speculate as being related to the signal seen in TP2005
492 $\delta^{14}\text{C}$.

493 With regard to the alignment of the palaeointensity and TP-2005 $\delta^{14}\text{C}$ signals, the Black
494 Sea and Tenaghi Philippon datasets can be unambiguously synchronised at the younger end of
495 the TP-2005 data via the presence of the C.I. isochron in both records. Our TP-2005 ^{14}C -derived
496 age of $39,556 \pm 310$ cal. BP for the C.I. (as modelled on to the Hulu Cave timescale;
497 $39,87739,165$ cal. BP, 95.4% highest probability density range; Fig. S5) is within statistical
498 agreement
499 (at 95.4% confidence) with the GICC05-implied age in the Black Sea record of 39,350 years
500 BP (Nowaczyk et al. 2012, 2013), providing additional support for the alignment of our TP2005
501 dataset with the Black Sea record at this point in time. We further note the statistical agreement
502 between our TP-2005 inferred age for the C.I. (at 95.4% confidence) with both the widely
503 quoted $^{40}\text{Ar}/^{39}\text{Ar}$ age of $39,230 \pm 110$ years BP (2σ) presented by De Vivo et al. (2001) and the
504 more recently published $^{40}\text{Ar}/^{39}\text{Ar}$ age of $39,850 \pm 140$ years BP (2σ) given by Giaccio et al.
505 (2017), noting that our TP-2005 inferred age falls centrally between these two $^{40}\text{Ar}/^{39}\text{Ar}$ age
506 estimates. Significantly, our TP-2005 inferred age for the C.I. on the IntCal13 timescale
507 ($38,725 \pm 239$ cal. BP; Fig. S5) is too young compared to these alternative age estimates (by
508 $\sim 1,100$ years as compared to the Giaccio et al. 2017 $^{40}\text{Ar}/^{39}\text{Ar}$ age). This provides further
509 support for the key finding above that IntCal13 is not accurate circa 40,000 years ago, and that
510 the Hulu Cave speleothem provides a better representation of the authentic radiocarbon
511 calibration curve at this point in time.

512

513

514 6. Conclusions

515

516 We have presented a record of atmospheric radiocarbon concentration ($\delta^{14}\text{C}$) from
517 Tenaghi Philippon core TP-2005 that provides a unique, continuous and direct (non-reservoir
518 corrected) record of $\delta^{14}\text{C}$ for the earliest ~10,000 years of the ^{14}C dating method. Our data
519 demonstrate higher frequency variability than the smoothed IntCal13 consensus calibration
520 curve (Reimer et al., 2013) or the recently published Hulu Cave speleothem dataset (Cheng et
521 al. 2018), yet lack the noise of the Lake Suigetsu dataset (Bronk Ramsey et al., 2012) or the
522 additional reservoir uncertainties of the marine (Fairbanks et al., 2005; Hughen et al., 2006)
523 and speleothem (Hoffmann et al., 2010; Cheng et al. 2018) datasets. Thus, we have been able
524 to compare $\delta^{14}\text{C}$ with the shared cosmogenic production signal of ^{10}Be in the Greenland ice
525 cores and direct palaeo-magnetic intensity records from the Black Sea (Nowaczyk et al., 2013)
526 and the GLOPIS-75 stack (Laj et al., 2004, 2014). These datasets demonstrate a similar pattern
527 in the build up to and through the principal peak of the Laschamp geomagnetic excursion. By
528 placing our ^{14}C dataset on to both the Hulu Cave U-series and IntCal13 timescales via Bayesian
529 statistical modelling, the comparison of our TP-2005 $\delta^{14}\text{C}$ dataset with these alternative records
530 also implicitly relates the underlying U-series, IntCal13 and GICC05 timescales themselves.
531 We suggest that, whilst the timescales are in broad agreement, the TP-2005 $\delta^{14}\text{C}$ data match
532 the Greenland ^{10}Be -inferred data more closely when modelled on to the Hulu Cave dataset
533 rather than the IntCal13 curve. This suggests that there is erroneous structure currently included
534 within the IntCal curve, which will be significantly improved upon with the addition of the
535 Hulu Cave dataset to the upcoming iteration of the IntCal calibration curve. It is unsurprising
536 that we would find erroneous structure within IntCal13 given that the underlying, contributing
537 ^{14}C datasets to IntCal are themselves in significant disagreement with each other at this time,
538 and we deem it most likely that the main error is incorporated from the climatically

539 wigglematched timescale of the Cariaco Basin dataset. Our TP-2005 data also suggest that there
540 is missing structure from the smoothed IntCal and Hulu Cave curves between circa 47,000 cal.
541 BP and 43,000 cal. BP. Thus, we provide a revised approximation of the authentic structure of
542 the radiocarbon calibration curve for the earliest ~10,000 years of the ^{14}C dating method, which
543 will have implications for all users of the technique over this time period.

544 **Acknowledgments:**

545

546 The authors would like to thank K. Christanis, S. Kalaitzidis and U. Müller for logistical and
547 technical support during the TP-2005 drilling campaign, as well as J. Graystone, M. Humm
548 and P. Leach at the Oxford Radiocarbon Accelerator Unit (ORAU) for running the ^{14}C samples
549 on the AMS. The ^{14}C dates were funded as part of the UK NERC (Natural Environment
550 Research Council)-funded project ‘RESET’ (Response of Humans to Abrupt Environmental
551 Transitions; grant number NE/E015670/1). RAS was supported by an Early Career Fellowship
552 from the Leverhulme Trust (ECF-2015-396). JP and AK acknowledge support through the
553 German Research Foundation (DFG). FA is supported by the Swedish Research council (VR
554 grant: 4.1-2016-00218). We would like to thank two anonymous reviewers for their
555 constructive comments on a previous version of our manuscript, and the editor, Prof Michael
556 Bickle, for facilitating the peer review process. This study is a contribution to the ‘INTIMATE’
557 (‘INTEgrating Ice-core, MARine and TERrestrial records for the period between 60,000 to 8000
558 years ago’) initiative (<http://intimate.nbi.ku.dk>).

559 **References:**

560

561 Adolphi F, Muscheler R (2016) Synchronizing the Greenland ice core and radiocarbon
562 timescales over the Holocene – Bayesian wiggle-matching of cosmogenic radionuclide records.
563 [Clim Past 12:15–30.](#)

564

565 Albert PG, Hardiman M, Keller J, Tomlinson EL, Smith VC, Bourne AJ, Wulf S, Zanchetta G,
566 Sulpizio R, Müller UC, Pross J, Ottolinnim L, Matthews IP, Blockley SPE, Menzies MA (2015)
567 Revisiting the Y-3 tephrostratigraphic marker: a new diagnostic glass geochemistry, age
568 estimate, and details on its climatostratigraphical context. [Quat Sci Rev 118:105-121](#).
569
570 Andersen KK, Svensson A, Johnsen SJ, Rasmussen SO, Bigler M, Röthlisberger R, Ruth U,
571 Siggaard-Andersen M-L, Steffensen JP, Dahl-Jensen D, Vinther BM, Clausen HB (2006) The
572 Greenland Ice Core Chronology 2005, 15-42 ka. Part 1: constructing the time scale. [Quat Sci](#)
573 [Rev 25:3246-3257](#).
574
575 Böhm E, Lippold J, Gutjahr M, Frank M, Blaser P, Antz B, Fohlmeister J, Frank N, Andersen
576 MB, Deininger M (2015) Strong and deep Atlantic meridional overturning circulation during
577 the last glacial cycle. [Nature 517:73-76](#).
578
579 Bonhommet N, Babkine, J (1967) Sur la présence d'aimantations inversées dans la Chaîne
580 des Puys, C.R. Acad. Sci. Paris, B 264:92-94.
581
582 Brauer A, Hajdas I, Blockley SPE, Bronk Ramsey C, Christl M, Ivy-Ochs S, Moseley GE,
583 Nowaczyk NN, Rasmussen SO, Roberts HM, Spötl C, Staff RA, Svensson A (2014) The
584 importance of independent chronology in integrating records of past climate change for the 608
585 ka INTIMATE time interval. [Quat Sci Rev 106:47-66](#).
586
587 Brock F, Higham T, Ditchfield P, Bronk Ramsey C (2010) Current pre-treatment methods for
588 AMS radiocarbon dating at the Oxford Radiocarbon Accelerator Unit (ORAU). [Radiocarbon](#)
589 [52:103-112](#).

590

591 Broecker WS, Gerard R, Ewing M, Heezen BC (1960) Natural radiocarbon in the Atlantic
592 Ocean. [J Geophys Res 65:2903-2931](#).

593

594 Bronk Ramsey C (2008) Deposition models for chronological records. [Quat Sci Rev 27:42-60](#).

595

596 Bronk Ramsey C (2009) Dealing with outliers and offsets in radiocarbon dating. [Radiocarbon](#)
597 [51:1023-1045](#).

598

599 Bronk Ramsey C (2019) OxCal ver.4.3, <https://c14.arch.ox.ac.uk/oxcal/OxCal.html>.

600

601 Bronk Ramsey C, Lee S (2013) Recent and planned developments of the program OxCal.
602 [Radiocarbon 55:720-730](#).

603

604 Bronk Ramsey C, Higham TFG, Leach P (2004) Towards high-precision AMS: progress and
605 limitations. [Radiocarbon 46:17-24](#).

606

607 Bronk Ramsey C, Dee M, Lee S, Nakagawa T, Staff RA (2010) Developments in the calibration
608 and modeling of radiocarbon dates. [Radiocarbon 52:953-961](#).

609

610 Bronk Ramsey C, Staff RA, Bryant CL, Brock F, Kitagawa H, van der Plicht J, Scholaut G,
611 Marshall MH, Brauer A, Lamb HF, Payne RL, Tarasov PE, Haraguchi T, Gotanda K,
612 Yonenobu H, Yokoyama Y, Tada R, Nakagawa T (2012) A complete terrestrial radiocarbon
613 record for 11.2-52.8 kyr BP. [Science 338:370-374](#).

614

615 Buizert C, Cuffey KM, Severinghaus JP, Baggenstos D, Fudge TJ, Steig EJ, Markle BR,
616 Winstrup M, Rhodes RH, Brook EJ, Sowers TA, Clow GD, Cheng H, Edwards RL, Sigl M,
617 McConnell JR, Taylor KC (2015) The WAIS Divide deep ice core WD2014 chronology – Part
618 1: Methane synchronization (68–31 kaBP) and the gas age–ice age difference. [Clim Past](#)
619 [11:153-173](#).

620

621 Cheng, H, Edwards, RL, Southon, J, Matsumoto, K, Feinberg, JM, Sinha, A, Zhou, W, Li, H,
622 Li, X, Xu, Y, Chen, S, Tan, M, Wang, Q, Wang, Y, Ning, Y (2018) Atmospheric $^{14}\text{C}/^{12}\text{C}$
623 changes during the last glacial period from Hulu Cave. [Science 362, 1293-1297](#).

624

625 Cox A (1969) Geomagnetic reversals. [Science 163:237-245](#).

626

627 De Vivo B, Rolandi G, Gans PB, Calvert A, Bohrson WA, Spera FJ, Belkin HE (2001) New
628 constraints on the pyroclastic eruptive history of the Campanian volcanic Plain (Italy). [Mineral](#)
629 [Petrology 73, 47-65](#).

630

631 Eggleston S, Schmitt J, Bereiter B, Schneider R, Fischer H (2016) Evolution of the stable
632 carbon isotope composition of atmospheric CO_2 over the last glacial cycle. [Paleoceanography](#)
633 [31:434-452](#).

634

635 Elsasser W, Ney EP, Winckler JR (1956) Cosmic ray intensity and geomagnetism. [Nature](#)
636 [178:1226-1227](#).

637

638 Fairbanks RG, Mortlock RA, Chiu T-C, Cao L, Kaplan A, Guilderson TP, Fairbanks TW,

639 Bloom AL, Grootes PM, Nadeau M-J (2005) Radiocarbon calibration curve spanning 0 to
640 50,000 years BP based on paired $^{230}\text{Th}/^{234}\text{U}/^{238}\text{U}$ and ^{14}C dates on pristine corals. [Quat Sci Rev](#)
641 [24:1781-1796](#).

642

643 Fletcher WJ, Müller UC, Koutsodendris A, Christanis K, Pross J (2013) A centennial-scale
644 record of vegetation and climate variability from 312 to 240 ka (Marine Isotope Stages 9c-a, 8
645 and 7e) from Tenaghi Philippon, NE Greece. [Quat Sci Rev 78:108-125](#).

646

647 Giaccio B, Hajdas I, Isaia R, Deino A, Nomade S (2017) High-precision ^{14}C and $^{40}\text{Ar}/^{39}\text{Ar}$
648 dating of the Campanian Ignimbrite (Y-5) reconciles the time-scales of climatic-cultural
649 processes at 40 ka. [Sci Rep 7:45940](#).

650

651 Grootes PM, Stuiver M, White JWC, Johnsen SJ, Jouzel J (1993) Comparison of oxygen
652 isotope records from the GISP2 and GRIP Greenland ice cores. [Nature 366:552-554](#).

653

654 Guillo H, Singer BS, Laj C, Kissel C, Scaillet S, Jicha BR (2004) On the age of the Laschamp
655 geomagnetic excursion. [Earth Planet Sci Lett 227:331-343](#).

656

657 Hajdas I, Taricco C, Bonani G, Beer J, Bernasconi SM, Wacker L (2011) Anomalous
658 radiocarbon ages found in Campanian Ignimbrite deposit of the Mediterranean deep-sea core
659 CT85-5. [Radiocarbon 53:575-583](#).

660

661 Herbst K, Muscheler R, Heber B (2017) The new local interstellar spectra and their influence
662 on the production rates of the cosmogenic radionuclides ^{10}Be and ^{14}C . *J Geophys Res Space*
663 *Phys* 122:23–34, <http://dx.doi.org/10.1002/2016JA023207>.

664

665 Higham TFG, Douka K, Wood RE, Bronk Ramsey C, Brock F, Basell L, Camps M,
666 Arrizabalaga A, Baena J, Barroso-Ruíz C, Bergman C, Boitard C, Boscato P, Caparrós M,
667 Conard NJ, Draily C, Froment A, Galván B, Gambassini P, Garcia-Moreno A, Grimaldi S,
668 Haesaerts P, Holt B, Iriarte-Chiapusso M-J, Jelinek A, Jordá Pardo JF, Maíllo-Fernández J-M,
669 Marom A, Maroto J, Menéndez M, Metz L, Morin E, Moroni A, Negrino F, Panagopoulou E,
670 Peresani M, Pirson S, de la Rasilla M, Riel-Salvatore J, Ronchitelli A, Santamaria D, Semal P,
671 Slimak L, Soler J, Soler N, Villaluenga A, Pinhasi R, Jacobi R (2014) The timing and
672 spatiotemporal patterning of Neanderthal disappearance. [Nature 512:306-309](#).
673
674 Hoffmann DL, Beck JW, Richards DA, Smart PL, Singarayer JS, Ketchmark T, Hawkesworth
675 CJ (2010) Towards radiocarbon calibration beyond 28 ka using speleothems from the Bahamas.
676 [Earth Planet Sci Lett 289:1-10](#).
677
678 Hogg AG, Turney CSM, Palmer JG, Southon J, Kromer B, Bronk Ramsey C, Boswijk G,
679 Fenwick P, Noronha A, Staff RA, Friedrich M, Reynard L, Guetter D, Wacker L, Jones RT
680 (2013) The New Zealand Kauri (*Agathis Australis*) Research Project: A radiocarbon
681 intercomparison of Younger Dryas wood and implications for IntCal13. [Radiocarbon](#)
682 [55:20352048](#).
683
684 Hughen KA, Southon JR, Lehman SJ, Bertrand C, Turnbull J (2006) Marine-derived ¹⁴C
685 calibration and activity record for the past 50,000 years updated from the Cariaco Basin. [Quat](#)
686 [Sci Rev 25:3216-3227](#).
687

688 Johnsen SJ, Clausen HB, Dansgaard W, Fuhrer K, Gundestrup N, Hammer CU, Iversen P,
689 Jouzel J, Stauffer B, Steffensen JP (1992) Irregular glacial interstadials recorded in a new
690 Greenland ice core. [Nature 359:311-313](#).

691

692 Laj C, Kissel C, Mazaud A, Channell JET, Beer J (2000) North Atlantic palaeointensity stack
693 since 75 ka (NAPIS-75) and the duration of the Laschamp event. [Phil Trans R Soc of Lond A](#)
694 [358:1009-1025](#).

695

696 Laj C, Kissel C, Beer J (2004) High Resolution Global Paleointensity Stack Since 75 kyr
697 (GLOPIS-75) Calibrated to Absolute Values. Timescales of the Paleomagnetic Field, eds
698 Channell JET, Kent DVK, Lowrie W, Meert JG (AGU Monogr. Ser. vol. 145) (Washington,
699 DC: American Geophysical Union), pp.255-265.

700

701 Laj C, Guillou H, Kissel C (2014) Dynamics of the earth magnetic field in the 10–75 kyr period
702 comprising the Laschamp and Mono Lake excursions: New results from the French Chaîne des
703 Puys in a global perspective. [Earth Planet Sci Lett 387:184-197](#).

704 Lal D, Peters B (1967) Cosmic ray produced radioactivity on the Earth. pp. 551-612 in Flüggé
705 S (ed.) [Handbuch für Physik](#). Springer, Berlin, Germany.

706

707 Lane CS, Brauer A, Blockley SPE, Dulski P (2013) Volcanic ash reveals time-transgressive
708 abrupt climate change during the Younger Dryas. [Geology 41:1251-1254](#).

709

710 McHargue LR, Damon PE (1991) The global beryllium 10 cycle. [Rev Geophys 29:141-158](#).

711

712 Müller UC, Pross J, Tzedakis PC, Gamble C, Kotthoff U, Schmiedl G, Wulf S, Christanis K
713 (2011) The role of climate in the spread of modern humans into Europe. [Quat Sci Rev](#)
714 [30:273279](#).

715

716 Muscheler R, Beer J, Wagner G, Laj C, Kissel C, Raisbeck GM, Yiou F, Kubik PW (2004)
717 Changes in the carbon cycle during the last deglaciation as indicated by the comparison of ^{10}Be
718 and ^{14}C records. [Earth Planet Sci Lett 219:325-340](#).

719

720 Muscheler R, Beer J, Kubik PW, Synal H-A (2005) Geomagnetic field intensity during the last
721 60,000 years based on ^{10}Be and ^{36}Cl from the Summit ice cores and ^{14}C . [Quat Sci Rev](#)
722 [24:1849-1860](#).

723

724 Muscheler R, Kromer B, Björck S, Svensson A, Friedrich M, Kaiser KF, Southon J (2008) Tree
725 rings and ice cores reveal ^{14}C calibration uncertainties during the Younger Dryas. [Nat](#)
726 [Geosci 1, 263-267](#).

727 Muscheler R, Adolphi F, Knudsen MF (2014a) Assessing the differences between the IntCal
728 and Greenland ice-core time scales for the last 14,000 years via the common cosmogenic
729 radionuclide variations. [Quat Sci Rev 106:81-87](#).

730

731 Muscheler R, Adolphi F, Svensson A (2014b) Challenges in ^{14}C dating towards the limit of the
732 method inferred from anchoring a floating tree ring radiocarbon chronology to ice core records
733 around the Laschamp geomagnetic field minimum. [Earth Planet Sci Lett 394:209-215](#).

734

735 Muscheler R, Adolphi F, Herbst K, Nilsson A (2016) The Revised Sunspot Record in
736 Comparison to Cosmogenic Radionuclide-Based Solar Activity Reconstructions. [Solar Phys](#)

737 [291:3025–3043](#).

738

739 NEEM Community Members (2013) Eemian interglacial reconstructed from a Greenland
740 folded ice core. [Nature 493:489-494](#).

741

742 NGRIP members (2004) High-resolution record of Northern Hemisphere climate extending
743 into the last interglacial period. [Nature 431:147-151](#).

744

745 Nowaczyk NR, Arz HW, Frank U, Kind J, Plessen B (2012) Dynamics of the Laschamp
746 geomagnetic excursion from Black Sea sediments. [Earth Planet Sci Lett 351-352:54-69](#).

747

748 Nowaczyk NR, Frank U, Kind J, Arz HW (2013) A high-resolution paleointensity stack of the
749 past 14 to 68 ka from Black Sea sediments. [Earth Planet Sci Lett 384:1-16](#).

750 Potgieter MS, Vos EE, Boezio M, De Simone N, Di Felice V, Formato V (2014) Modulation
751 of Galactic Protons in the Heliosphere During the Unusual Solar Minimum of 2006 to 2009.
752 *Sol Phys* 289:391-406, <http://dx.doi.org/10.1007/s11207-013-0324-6>.

753

754 Pross J, Tzedakis P, Schmiedl G, Christanis K, Hooghiemstra H, Müller UC, Kotthoff U,
755 Kalaitzidis S, Miller A (2007) Tenaghi Philippon (Greece) Revisited: Drilling a Continuous
756 Lower-Latitude Terrestrial Climate Archive of the Last 250,000 Years. [Scientific Drilling 5:44-](#)
757 [46](#).

758

759 Pross J, Kotthoff U, Müller UC, Peyron O, Dormoy I, Schmiedl G, Kalaitzidis S, Smith AM
760 (2009) Massive perturbation in terrestrial ecosystems of the Eastern Mediterranean region
761 associated with the 8.2 kyr BP climatic event. [Geology 37:887-890](#).

762

763 Pross J, Koutsodendris A, Christanis K, Fischer T, Fletcher WJ, Hardiman M, Kalaitzidis S,
764 Knipping M, Kotthoff U, Milner AM, Müller UC, Schmiedl G, Siavalas G, Tzedakis PC, Wulf
765 S (2015) The 1.35-Ma-long terrestrial climate archive of Tenaghi Philippon, northeastern
766 Greece: Evolution, exploration, and perspectives for future research. [Newsl Stratigr 48:253276](#).

767

768 Rasmussen SO, Andersen KK, Svenson AM, Steffensen JP, Vinther BM, Johnsen SJ, Clausen
769 HB, Larsen LB, Bigler M, Röthlisberger R, Andersen M-LS, Fisher H, Ruth U, Goto-Azuma
770 K, Hansson M (2006) A new Greenland ice core chronology for the last glacial termination. [J
771 Geophys Res Atmos 111:D06102](#).

772 Reimer PJ, Bard E, Bayliss A, Beck JW, Blackwell PG, Bronk Ramsey C, Buck CE, Edwards
773 RL, Friedrich M, Grootes PM, Guilderson TP, Haflidason H, Hajdas I, Hatté C, Heaton TJ,
774 Hoffmann DL, Hogg AG, Hughen KA, Kaiser KF, Kromer B, Manning SW, Niu M, Reimer
775 RW, Richards DA, Scott EM, Southon JR, Staff RA, Turney CSM, van der Plicht J (2013)
776 IntCal13 and Marine13 radiocarbon age calibration curves 0-50,000 years cal BP. [Radiocarbon
777 55:1869-1887](#).

778

779 Sanchez Goñi MF, Harrison SP (2010) Millennial-scale climate variability and vegetation
780 changes during the Last Glacial: Concepts and terminology. [Quat Sci Rev 29:2823-2827](#).

781

782 Seierstad IK, Abbott PM, Bigler M, Blunier T, Bourne AJ, Brook E, Buchardt SL, Buizert C,
783 Clausen HB, Cook E, Dahl-Jensen D, Davies SM, Guillevic M, Johnsen SJ, Pedersen DS, Popp
784 TJ, Rasmussen SO, Severinghaus JP, Svensson A, Vinther BM (2014) Consistently dated
785 records from the Greenland GRIP, GISP2 and NGRIP ice cores for the past 104 ka reveal

786 regional millennial-scale $\delta^{18}\text{O}$ gradients with possible Heinrich event imprint, [Quat Sci Rev](#)
787 [106:29-46](#).

788

789 Siegenthaler U, Heimann M, Oeschger H (1980) ^{14}C variations caused by changes in the global
790 carbon cycle. [Radiocarbon 22:177-191](#).

791

792 Sigl M, Winstrup M, McConnell JR, Welten KC, Plunkett G, Ludlow F, Büntgen U, Caffee M,
793 Chellman N, Dahl-Jensen D, Fischer H, Kipfstuhl S, Kostick C, Maselli OJ, Mekhaldi F,
794 Mulvaney R, Muscheler R, Pasteris DR, Pilcher JR, Salzer M, Schüpbach S, Steffensen JP,
795 Vinther BM, Woodruff TE (2015), Timing and climate forcing of volcanic eruptions for the
796 past 2,500 years. [Nature 523:543-549](#).

797

798 Singer BS, Guillou H, Jicha BR, Laj C, Kissel C, Beard BL, Johnson CM (2009) $^{40}\text{Ar}/^{39}\text{Ar}$, K–
799 Ar and ^{230}Th – ^{238}U dating of the Laschamp excursion: A radioisotopic tie-point for ice core and
800 climate chronologies. [Earth Planet Sci Lett 286:80-88](#).

801

802 Southon J, Noronha AL, Cheng H, Edwards RL, Wang Y (2012) A high-resolution record of
803 atmospheric ^{14}C based on Hulu Cave speleothem H82. [Quat Sci Rev 33:32-41](#).

804

805 Staff RA, Bronk Ramsey C, Bryant CL, Brock F, Payne RL, Schlolaut G, Marshall MH, Brauer
806 A, Lamb HF, Tarasov P, Yokoyama Y, Haraguchi T, Gotanda K, Yonenobu H, Nakagawa T,
807 Suigetsu 2006 project members (2011) New ^{14}C determinations from Lake Suigetsu, Japan:
808 12,000 to 0 cal BP. [Radiocarbon 53:511-528](#).

809

810 Staff RA, Reynard L, Brock F, Bronk Ramsey C (2014) Wood Pretreatment Protocols and
811 Measurement of Tree-Ring Standards at the Oxford Radiocarbon Accelerator Unit (ORAU).
812 [Radiocarbon 56:709-715](#).
813
814 Steffensen JP, Andersen KK, Bigler M, Clausen HB, Dahl-Jensen D, Fischer H, Goto-Azuma
815 K, Hansson M, Johnsen SJ, Jouzel J, Masson-Delmotte V, Popp T, Rasmussen SO,
816 Röthlisberger R, Ruth U, Stauffer B, Siggaard-Andersen M-L, Sveinbjörnsdóttir AE, Svensson
817 A, White JWC (2008) High-Resolution Greenland Ice Core Data Show Abrupt Climate Change
818 Happens in Few Years. [Science 321:680-684](#).
819
820 Svensson A, Andersen KK, Bigler M, Clausen HB, Dahl-Jensen D, Davies SM, Johnsen SJ,
821 Muscheler R, Parrenin F, Rasmussen SO, Röthlisberger R, Seierstad I, Steffensen JP, Vinther,
822 BM (2008) A 60 000 year Greenland stratigraphic ice core chronology. [Clim. Past 4, 47-57](#).
823
824 Turney CSM, Fifield LK, Hogg AG, Palmer JG, Hughen K, Baillie MGL, Galbraith R, Ogden
825 J, Lorrey A, Tims SG, Jones RT (2010) The potential of New Zealand kauri (*Agathis australis*)
826 for testing the synchronicity of abrupt climate change during the Last Glacial Interval
827 (60,000-11,700 years ago). [Quat Sci Rev 29:3677-3682](#).
828
829 Turney CSM, Palmer JG, Bronk Ramsey C, Adolphi F, Muscheler R, Hughen KA, Staff RA,
830 Jones RT, Thomas ZA, Fogwill CJ, Hogg AG (2016) High-precision dating and correlation of
831 ice, marine and terrestrial sequences spanning Heinrich Event 3: Testing mechanisms of
832 interhemispheric change using New Zealand ancient kauri (*Agathis australis*). [Quat Sci Rev](#)
833 [137:126-134](#).
834

835 Tzedakis PC, Hooghiemstra H, Pälike H (2006) The last 1.35 million years at Tenaghi
836 Philippon: revised chronostratigraphy and long-term vegetation trends. [Quat Sci Rev](#)
837 [25:34163430](#).

838

839 Valet J-P, Meynadier L (1993) Geomagnetic field intensity and reversals during the past four
840 million years. [Nature 366:234-238](#).

841

842 Vinther BM (2008) A 60 000 year Greenland stratigraphic ice core chronology. [Clim Past 4:47-](#)
843 [57](#).

844

845 Voelker AHL, Grootes PM, Nadeau M-J, Sarnthein M (2000) Radiocarbon levels in the Iceland
846 Sea from 25-53 kyr and their link to the Earth's magnetic field intensity. [Radiocarbon](#)
847 [42:437452](#).

848

849 Wijmstra TA (1969) Palynology of the first 30 metres of a 120 m deep section in northern
850 Greece. [Acta Botanica Neerlandica 18:511-527](#).

851

852 Wulf S, Hardiman MJ, Staff RA, Koutsodendris A, Appelt O, Blockley SPE, Lowe JJ, Manning
853 CJ, Ottolini L, Schmitt AK, Smith VC, Tomlinson EL, Vakhrameeva P, Knipping M, Kotthoff
854 U, Milner AM, Müller UC, Christanis K, Kalaitzidis S, Tzedakis PC, Schmiedl G, Pross J
855 (2018) The Marine Isotope Stage 1–5 cryptotephra record of Tenaghi Philippon, Greece:
856 towards a detailed tephrostratigraphic framework for the Eastern Mediterranean region. [Quat](#)
857 [Sci Rev 186, 236-262](#)

858

859 Yiou F, Raisbeck, GM, Baumgartner S., Beer J, Hammer C, Johnsen S, Jouzel J, Kubik PW,
860 Lestringuéz J, Stiévenard M, Suter M, Yiou P (1997) Beryllium 10 in the Greenland Ice Core

861 Project ice core at Summit, Greenland. [J Geophys Res 102:26783-26794](https://doi.org/10.1029/2012JG001994).

862 **Figure Captions:**

863

864 **Fig. 1.** Location of the Tenaghi Philippon site, Eastern Macedonia, NE Greece. Inset shows the

865 location of sediment core TP-2005 within the Drama Basin.

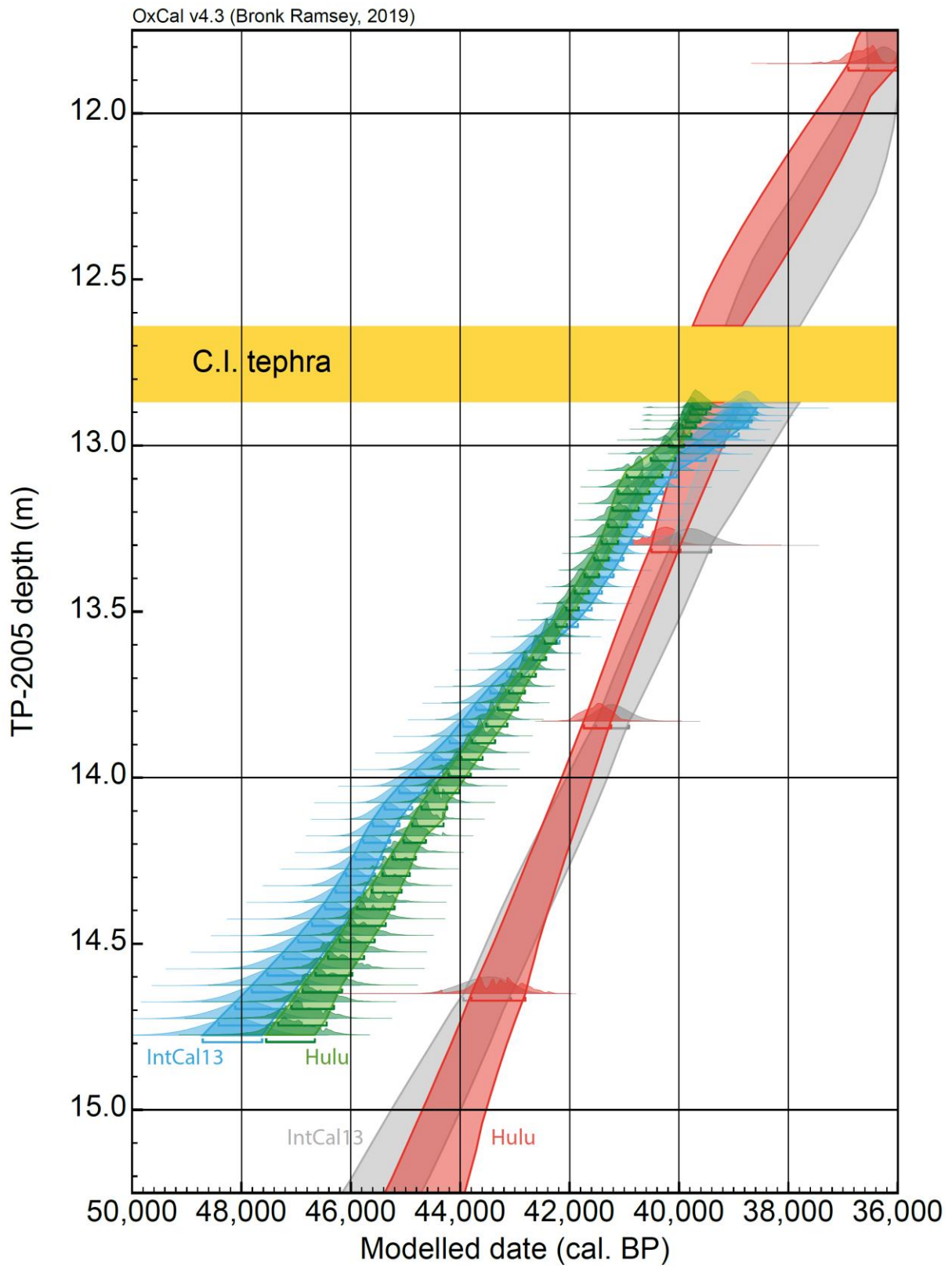


866

867

868 **Fig. 2.** Revised age-depth profile (green) for core TP-2005 from Tenaghi Philippon, as
869 compared to the previously published dataset of Müller et al. (2011; red), generated by
870 independent **P_Sequence** deposition modelling in OxCal ver.4.3 (Bronk Ramsey, 2008,
871 2019; Bronk Ramsey and Lee, 2013) on to the Hulu Cave ¹⁴C calibration dataset of Cheng et
872 al. (2018). Equivalent age-depth profiles are additionally plotted for the same TP-2005 datasets
873 (this study, blue; and Müller et al., 2011, grey) as modelled on to the IntCal13 calibration curve
874 (Reimer et al., 2013). Modelled probability density functions are plotted with the 68.2% highest
875 probability density range interpolations overlain. For the unmodelled data, see Supplementary
876 Figure S3.

877



878

879 **Fig. 3.** Comparison of the shared production signals of the cosmogenic nuclides ^{14}C and ^{10}Be

880 with relative palaeointensity. (a) NGRIP $\delta^{18}\text{O}$ (NGRIP members, 2004; light blue data series);

881 **(b)** Inferred $\delta^{14}\text{C}$ from the GLOPIS-75 stack (Laj et al., 2004, 2014; blue data series) and Black
882 Sea (Nowaczyk et al., 2013; as ‘tuned’ to GICC05, red data series) relative palaeointensity
883 datasets; **(c)** Inferred $\delta^{14}\text{C}$ from Greenland ^{10}Be flux (Yiou et al., 1997; Muscheler et al., 2004,
884 2014b); **(d)** Reconstructed atmospheric ^{14}C concentrations ($\delta^{14}\text{C}$) based on Tenaghi Philippon
885 core TP-2005 (dark green data points; this paper), as well as the kauri dataset of Turney et al.
886 (2010; purple data series), as modelled against the Hulu Cave ^{14}C calibration dataset (Cheng et
887 al., 2018; pink curve); **(e)** Reconstructed atmospheric ^{14}C concentrations ($\delta^{14}\text{C}$) based on
888 Tenaghi Philippon core TP-2005 (dark green data points; this paper) as modelled against
889 IntCal13 (red curve). For comparison, the Lake Suigetsu (Bronk Ramsey et al., 2012) (blue
890 dataset) is additionally plotted. For clarity, all data are plotted at 68.2%/1 σ probability ranges.
891 (a-c) are all plotted on the GICC05 timescale BP (Andersen et al., 2006; Rasmussen et al.,
892 2006; Svensson et al., 2008); (d) is plotted on the Hulu Cave U-series timescale; and (e) is
893 plotted on the IntCal13 cal. BP timescale. Additionally, the shaded light blue boxes mark the
894 approximate timings of Heinrich stadials HS4 and HS5 (Sanchez Goñi and Harrison, 2010);
895 the hashed brown line marks the position of the Campanian Ignimbrite (C.I.) tephra in the
896 Tenaghi Philippon and Black Sea records.

